ISSN 1674-1056
http://cpb.iphy.ac.cn
http://iopscience.iop.org/cpb
中国物理 B
Chinese Physics
中国物理
Chinese Physics B

A broadband cross-polarization conversion anisotropic metasurface based on multiple plasmon resonances

M Ismail Khan, Farooq A Tahir
Citation: Chin. Phys. B . 2018, 27(1): 014101. **doi:** 10.1088/1674-1056/27/1/014101

Journal homepage: http://cpb.iphy.ac.cn; http://iopscience.iop.org/cpb

What follows is a list of articles you may be interested in

An electrically tunable metasurface integrated with graphene for mid-infrared light modulation

Zongpeng Wang(王宗鹏), Ya Deng(邓娅), LianFeng Sun(孙连峰)
Chin. Phys. B . 2017, 26(11): 114101. **doi:** 10.1088/1674-1056/26/11/114101

Ultra-wideband RCS reduction using novel configured chessboard metasurface

Ya-Qiang Zhuang(庄亚强), Guang-Ming Wang(王光明), He-Xiu Xu(许河秀)
Chin. Phys. B . 2017, 26(5): 054101. **doi:** 10.1088/1674-1056/26/5/054101

Ultra-thin two-dimensional transmissive anisotropic metasurfaces for polarization filter and beam steering application

Wen-Long Guo(郭文龙), Guang-Ming Wang(王光明), Hai-Peng Li(李海鹏), Kun Zhang(张昆), Tong Cai(蔡通)
Chin. Phys. B . 2016, 25(10): 104101. **doi:** 10.1088/1674-1056/25/10/104101

Ultra-thin single-layer transparent geometrical phase gradient metasurface and its application to high-gain circularly-polarized lens antenna

Tang-Jing Li(李唐景), Jian-Gang Liang(梁建刚), Hai-Peng Li(李海鹏), Ya-Qiao Liu(刘亚峤)
Chin. Phys. B . 2016, 25(9): 094101. **doi:** 10.1088/1674-1056/25/9/094101

Utra-thin anisotropic transmitting metasurface for polarization beam splitter application

Wen-Long Guo(郭文龙), Guang-Ming Wang(王光明), Shan-Shan Ding(丁姗姗), Hai-Peng Li(李海鹏), Tong Cai(蔡通)
Chin. Phys. B . 2016, 25(8): 084101. **doi:** 10.1088/1674-1056/25/8/084101

A broadband cross-polarization conversion anisotropic metasurface based on multiple plasmon resonances

M Ismail Khan[1,2], and Farooq A Tahir[1,†]

[1] Research Institute for Microwave and Millimeter-wave Studies (RIMMS), National University of Sciences and Technology (NUST), Islamabad, Pakistan
[2] Department of Electrical Engineering, COMSATS Institute of Information Technology, Attock Campus, Pakistan

(Received 30 May 2017; revised manuscript received 25 July 2017; published online 28 November 2017)

A compact broadband cross-polarization conversion metasurface functioning in the microwave regime is realized and experimentally demonstrated. The metasurface consists of a two-dimensional periodic arrangement of anisotropic double-slit split-ring-resonator-based unit cells printed on top of a dielectric substrate, backed by metallic cladding. The proposed metasurface converts an *x*- or *y*-polarized wave into its orthogonal polarization over a fractional bandwidth of 100% from 5–15 GHz, both for normal as well as oblique incidence. Moreover, the sub-wavelength unit-cell size, thin dielectric substrate, and unique unit-cell design collectively make the response of the metasurface same for both polarizations and insensitive to the incidence angle. The designed structure is fabricated and tested. The measurement and simulation results are found to be consistent with each other.

Keywords: cross-polarization conversion, anisotropy, metasurface, plasmon resonances

PACS: 41.20.Jb **DOI:** 10.1088/1674-1056/27/1/014101

1. Introduction

Control and manipulation of the polarization state of electromagnetic (EM) waves has always been of profound interest in the scientific communities due to its fundamental role in a wide range of applications including contrast imaging microscopy, optical sensing, molecular biotechnology, and microwave communication. Conventional techniques can be applied for polarization control using natural materials, such as the optical activity of crystals, Faraday effect, gases or solutions of chiral molecules (e.g., sugars), proteins with helical secondary structure, and chiral liquid crystals.[1] Such methods generally result in bulky volumes, narrow bandwidth, and an incidence-angle-dependent response which greatly limits their use in practical applications. Artificial structures must be realized to develop miniaturized polarization control devices with wide bandwidths and angularly stable responses.

The most famous artificial electromagnetic structures are the engineered structures called metamaterials[2,3] that utilize the periodic sub-wavelength patterning to create an effective macroscopic response not found in natural materials. A two-dimensional analog of metamaterial, called metasurface[4,5] has received increased attention for polarization control of EM waves. In recent years, anisotropic[6–10] and chiral metamaterials[11] (metamaterials lacking mirror symmetry) - based metasurfaces have attracted much interest. They have been extensively investigated in terms of linear[12–14] or circular polarizers[15–19] and asymmetric transmission[20–22] for their unique electromagnetic characteristics, such as elliptical or circular dichroism, bi-anisotropy, and magneto-electric coupling.

Although many metamaterial-based designs[12,23,24] achieve excellent polarization conversion efficiencies over much smaller distances compared to the wavelength, these designs only work for very narrow bandwidths. There are two main methods to extend the polarization conversion bandwidth. The first is to stack the metallo-dielectric multilayers. Using a multilayer metallo-dielectric structure composed of twisted complementary split-ring resonators,[25] wide-band polarization conversion is achieved over an operating frequency band 9.8–12.5 GHz. The multilayer approach usually makes the design bulkier and difficult to fabricate. The second method is to enhance the bandwidth and to properly design the unit cell so that it can produce multiple plasmonic resonances. A reflective broadband (2–3.5 GHz) 90° polarization rotator was realized[26] using multi-order plasmon resonances. Similarly, using asymmetric double split-ring resonators, broadband (9.1–12.9 GHz) polarization conversion is achieved[27] through multiple electric and magnetic plasmon resonances. A double-head arrow structure[28] is employed to achieve ultra-wideband polarization conversion using four plasmonic resonances. There are other broadband designs[29,30] recently proposed in the literature; however, the main limitations of these designs are that they only achieve polarization conversion for normal incidence and do not act as a polarization rotator for oblique incidence. To realize an electrically thin, broadband metasurface with a polarization conversion efficiency that is also independent of the incidence angle is a very challenging task.

In this work, an electrically thin ($0.08\lambda_o$, where λ_o is the free space wavelength at 10 GHz) and ultra-broadband reflec-

†Corresponding author. E-mail: farooq.tahir@seecs.edu.pk

© 2018 Chinese Physical Society and IOP Publishing Ltd

tive cross-polarization-conversion (CPC) anisotropic metasurface, working not only for normal but also for oblique incidence, is proposed. The proposed design achieved cross-polarization-conversion due to its anisotropic magnetic response along both u and v-axes and obtained its broadband operation through three plasmonic resonances. Owing to the sub-wavelength unit cell size, thin dielectric substrate, and optimized design of the unit cell, the response of the metasurface is insensitive to the incidence angle and is the same for both polarizations.

2. Design and analysis

2.1. Geometrical configuration

A generalized schematic diagram of the CPC metasurface is depicted in Fig. 1(a).

It consists of a two-dimensional periodic array of metallic split-ring-resonator (SRR) unit cells inside which a square metallic loop is placed co-centrically, as shown in the unit cell depiction of Fig. 1(b). The SRRs have two equal gap slits placed in the middle of the perpendicular sides. The two-dimensional periodic array of the SRRs and loops is designed over a dielectric substrate backed by a metallic ground plane. The unit cells are repeated in the x and y directions with the same periodicity of 7 mm. A 3D schematic of the unit cell is shown in Fig. 1(c). Figure 1(d) shows a photograph of the fabricated prototype which consisted of 44×44 unit cells.

CPC implies that an incident x-polarized electromagnetic wave is converted into a y-polarized wave, and vice versa, upon reflection from the metasurface. The reflected field generally consists of both the x and y components, even when the incident field has only one component. The co-polarized reflection coefficients are defined as: $R_{xx} = |E_{\mathrm{rx}}|/|E_{\mathrm{ix}}|$ and $R_{yy} = |E_{\mathrm{ry}}|/|E_{\mathrm{iy}}|$ while the cross-polarized reflection coefficients are: $R_{yx} = |E_{\mathrm{ry}}|/|E_{\mathrm{ix}}|$ and $R_{xy} = |E_{\mathrm{rx}}|/|E_{\mathrm{iy}}|$. R_{yx} is the reflection coefficient when the incident field E_{i} is x-polarized while the reflected field E_{r} is y-polarized, and R_{xy} is the reflection coefficient when the incident field is y-polarized while the reflected field is x-polarized.

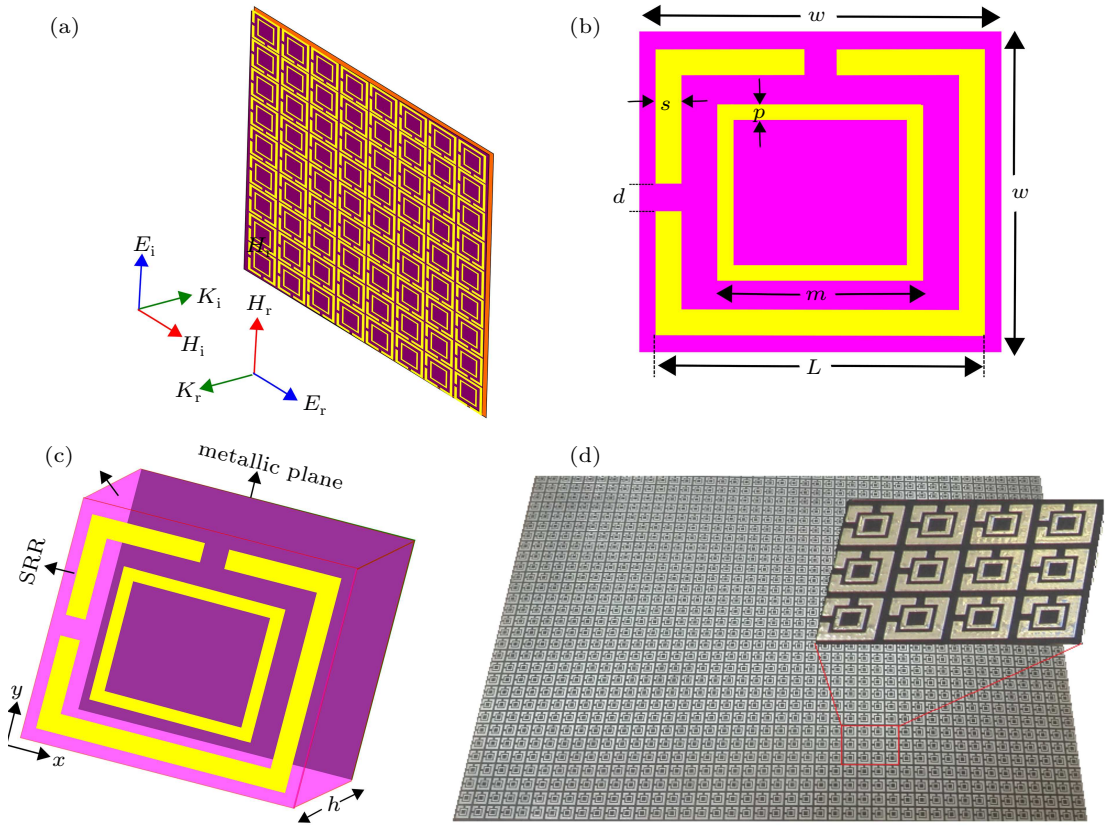


Fig. 1. (color online) (a) Schematic diagram of the proposed metasurface. (b) Unit cell. (c) 3D schematic of the unit cell. (d) Photograph of the real fabricated metasurface sample.

2.2. Operating principle

The metasurface consists of a repetition of sub-wavelength unit cells which can be polarized electrically or magnetically; therefore, an arbitrary metasurface can be modeled as a surface consisting of polarizable particles or artificial atoms.[31] Each particle can be characterized by its electric and magnetic polarizability ($\alpha_{\mathrm{e,m}}$). The electric and magnetic polarizability of the particles is the ratio of the electric and magnetic dipole moments to the respective local average

electric and magnetic fields. The electric and magnetic dipole moments can be related to the average electric and magnetic fields via

$$\begin{bmatrix} \boldsymbol{p} \\ \boldsymbol{m} \end{bmatrix} = \begin{bmatrix} \alpha_{\rm ee} & \alpha_{\rm em} \\ \alpha_{\rm me} & \alpha_{\rm mm} \end{bmatrix} \begin{bmatrix} \boldsymbol{E} \\ \boldsymbol{H} \end{bmatrix}, \tag{1}$$

where $\boldsymbol{p} = [p_x, p_y]^{\rm T}$ is the electric dipole moment, $\boldsymbol{m} = [m_x, m_y]^{\rm T}$ is the magnetic dipole moment, and $\boldsymbol{E} = [E_x, E_y]^{\rm T}$ and $\boldsymbol{H} = [H_x, H_y]^{\rm T}$ represent the average tangential electric and magnetic fields at the metasurface, respectively. The time changing electric and magnetic polarization will cause electric and magnetic surface currents on the metasurface given by

$$\begin{bmatrix} \boldsymbol{J} \\ \boldsymbol{M} \end{bmatrix} = {\rm i}\omega \begin{bmatrix} \alpha_{\rm ee} & \alpha_{\rm em} \\ \alpha_{\rm me} & \alpha_{\rm mm} \end{bmatrix} \begin{bmatrix} \boldsymbol{E} \\ \boldsymbol{H} \end{bmatrix}, \tag{2}$$

where $\boldsymbol{J} = [J_x, J_y]^{\rm T}$ and $\boldsymbol{M} = [M_x, M_y]^{\rm T}$ are the electric and magnetic surface current densities, respectively, and ω is the angular frequency of the incident electromagnetic wave. A time harmonic form of $e^{{\rm i}\omega t}$ is considered here. The electric and magnetic response determines the impedance of the metasurface given by $\eta(\omega) = \sqrt{\frac{\mu(\omega)}{\varepsilon(\omega)}}$, where $\eta(\omega)$ is the frequency-dependent impedance, $\mu(\omega)$ and $\varepsilon(\omega)$ are the frequency-dependent magnetic and electric permittivities, respectively. The reflection coefficient at normal incidence is given by

$$R(\omega) = \frac{\eta(\omega) - \eta_{\rm o}}{\eta(\omega) + \eta_{\rm o}}, \tag{3}$$

where $R(\omega)$ is the frequency dependent complex reflection coefficient consisting of both real and imaginary parts, $\eta_{\rm o}$ is the impedance of free space and is 377 Ω. The reflection coefficient can be expressed in its magnitude and phase form as $|R(\omega)|\,e^{{\rm i}\phi(\omega)}$, where $\phi(\omega)$ is the phase of the reflection coefficient which also depends upon the frequency of the incident electromagnetic wave.

Equation (3) shows that if the impedance of the metasurface in an electromagnetic spectrum is much larger than the free space impedance $\eta_{\rm o}$, then the magnitude of the reflection coefficient is unity and its phase is 0°. In such an electromagnetic spectrum, the metasurface behaves as a high-impedance surface (HIS),[32] also called an artificial magnetic conductor (AMC), which ideally reflects the electromagnetic wave with a magnitude of unity and zero phase. To understand the CPC upon reflection from the metasurface, consider a y-polarized plane electromagnetic wave incident normally on the metasurface as shown in Fig. 2.

As can be seen from Fig. 2, the unit cell is anisotropic along the u- and v-axes which are at ±45° to the x- and y-axes. The unit cell also has mirror symmetry along the v-axis making the structure achiral.[33] The incident electric field can be decomposed into u and v components and $\boldsymbol{E}_{\rm i} = \hat{\boldsymbol{u}} E_{{\rm i}u}\, e^{{\rm i}\varphi} + \hat{\boldsymbol{v}} E_{{\rm i}v}\, e^{{\rm i}\varphi}$. The reflected electric field can be expressed as:

$$\boldsymbol{E}_{\rm r} = \hat{\boldsymbol{u}} R_u E_{{\rm i}u}\, e^{{\rm i}\varphi} + \hat{\boldsymbol{v}} R_v E_{{\rm i}v}\, e^{{\rm i}\varphi},$$

where $\boldsymbol{R}_u = |R_u|\, e^{{\rm i}\phi_u} = E_{{\rm r}u}/E_{{\rm i}u}$ and $R_v = |R_v|\, e^{{\rm i}\phi_v} = E_{{\rm r}v}/E_{{\rm i}v}$ are the complex reflection coefficients. If in a certain frequency range $|R_u| \approx |R_v| \approx 1$ and one component of the incident wave is reflected in phase (a phase difference of $\Delta\phi \approx 0°$) with the component of the incident electric field along the same axis, while the other orthogonal component is reflected out of phase ($\Delta\phi \approx 180°$) then the electric field of the reflected wave is rotated 90° with respect to the electric field of the incident wave. In other words, CPC is achieved and the incident y-polarized wave is reflected as the x-polarized wave as shown in Fig. 2.

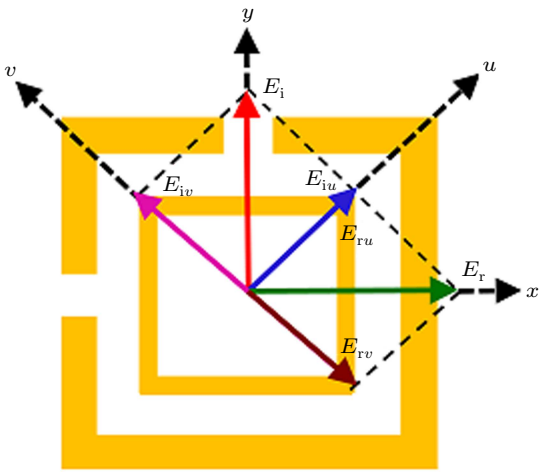


Fig. 2. (color online) Incident electric field along the y-axis is decomposed into two orthogonal components along the u- and v-axes and reflected along the x-axis.

2.3. Simulation results

The metasurface shown in Fig. 1 was demonstrated with electromagnetic modeling and full-wave numerical simulations using Ansys HFSS. The optimized physical dimensions (in millimeters) of the final design are: $w = 7$, $L = 6$, $s = 1$, $p = 0.5$, $d = 1$, $m = 3$, and $h = 2.4$. The dielectric substrate was FR4 with a relative permittivity of 4.4 and loss tangent of 0.02. Copper with a conductivity of 5.8×10^7 S/m was used for the SRRs and metallic ground plane.

The co- and cross-polarized reflection coefficients under normal incidence when the incident wave was x-polarized (TM polarization) are shown in Fig. 3(a). As can be seen from Fig. 3(a), resonances occurr at 5.4, 7.6, and 12.4 GHz, where the cross-polarized reflection approaches 0 dB (unity magnitude) while the co-polarized reflection coefficient reaches to a minimum value of −27 dB. Therefore, at resonance frequencies, an incident x-polarized wave is completely converted into a y-polarized wave upon reflection from the metasurface.

Figure 3(b) shows the co- and cross-polarized reflection coefficients for normal incidence when the incident field is y-polarized (TE polarization). Similar to the case of the x-polarized waves, the co-polarized reflection is minimized to −18, −26, and −28 dB at the three resonances 5.4, 7.6, and

12.4 GHz, respectively, while the cross-polarized reflection approaches 0 dB. It can be seen from Figs. 3(a) and 3(b) that the cross-polarized reflection coefficient is larger than −3 dB over a wide frequency range 5–15 GHz leading to a fractional bandwidth of 100%. It is also clear from Fig. 3 that the response of the metasurface is the same for both the *x*- and *y*-polarized waves. Both of these polarizations are converted into their respective cross-polarized waves in a similar fashion. Moreover, the resonances are achieved at the same three distinct frequencies for both polarizations. This same polarization conversion behavior for both the *x*- and *y*-polarization results from the mirror symmetry of the unit cell along the *v*-axis, in which the structure appears the same to both the *x*- and *y*-polarizations (both of these encounter the split-bearing and no-split sides of the SRR).

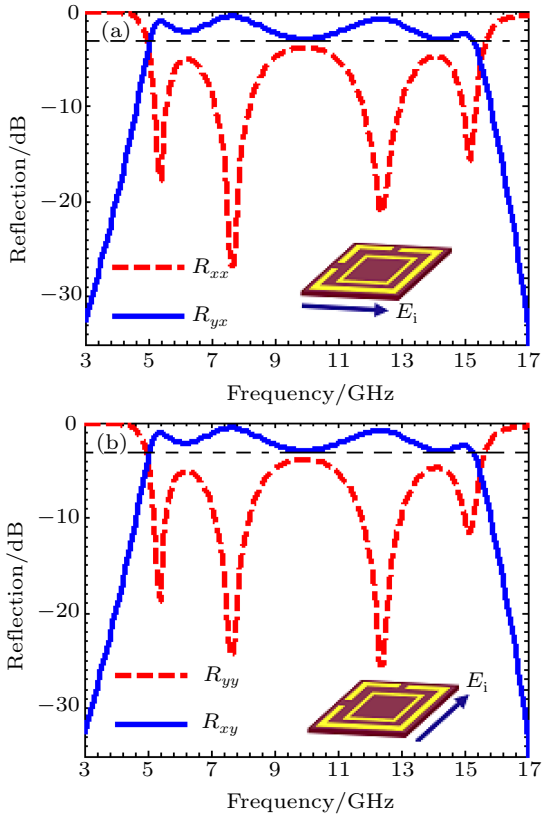


Fig. 3. (color online) Co- and cross-polarized reflection coefficients when the incident field is (a) *x*-polarized and (b) *y*-polarized.

In order for the CPC metasurface to be useful in a variety of applications, the response of the metasurface must be stable against variations in the incidence angle. A metasurface based on a relatively thin dielectric substrate has a higher angular stability compared with one employing a thick substrate, however, thin substrates result in a narrower bandwidth.[34,35] Dielectric substrates with large dielectric constants can be used to enhance angular stability, however, this also reduces the bandwidth.[34,35] A possible way to achieve both broad bandwidth and an angularly stable response is to design a unit cell with a sub-wavelength size and unique structural configuration so that it can produce multiple plasmonic resonances. The co- and cross-polarized reflection coefficients for different incidence angles when the incident field is *x*-polarized (TM polarization) are shown in Figs. 4(a) and 4(b). As it can be

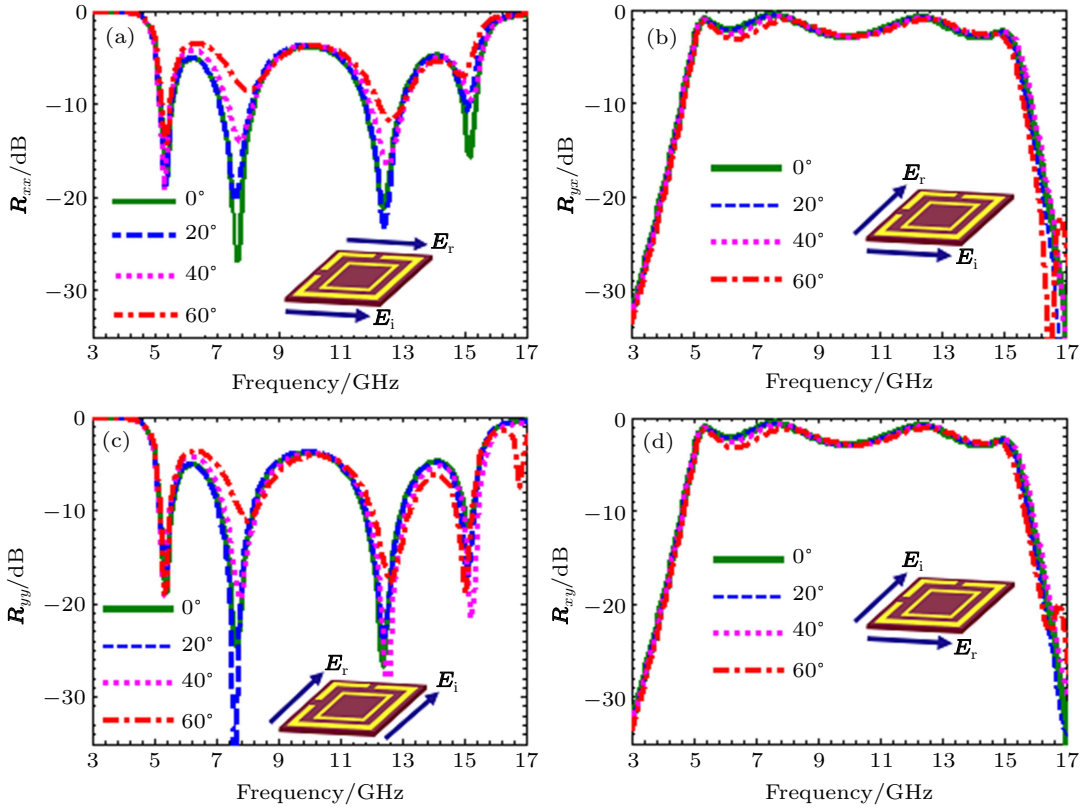


Fig. 4. (color online) Reflection coefficient when the incident and reflected fields are *y*-polarized: (a) Co-polarized and (b) cross-polarized.

seen from Fig. 4(b), the cross-polarized reflection is quite stable against variations in the incidence angle. The incidence angles had little effect on both the performance and bandwidth of the metasurface. The co- and cross-polarized reflection coefficients when the incident wave is *y*-polarized (TE polarization) for different incidence angles, are presented in Figs. 4(c) and 4(d), respectively. As the incident waves are transverse magnetic (TM) polarized, the small variations in the cross-polarized reflection are due to the electric field which started passing into the SRR and loop at large incidence angles and disturbes the current flow. However, these variations remain in an acceptable range due to the surface currents on the SRR and the loop which counteract against the effects induced by the oblique incidence, and hence stabilized the response. Generally, the stability of the response of the metasurface against variations in the incidence angle results from the unique optimized design of the unit cell, thin dielectric substrate (0.12λ at 15 GHz), and sub-wavelength unit cell size which are 0.11λ at 5 GHz and 0.35λ at 15 GHz. As in most applications, the incoming wave can have any arbitrary incidence angle; therefore, the incidence angle insensitivity makes the proposed metasurface a potential candidate for many practical applications.

2.4. Physical mechanism

To understand the physical mechanism responsible for the CPC, the proposed design is analyzed under *u* and *v* polarizations to study the magnitude and phase of the reflection coefficient, as well as surface current distribution. The magnitude and phase of the reflection coefficient for the *u* and *v*-polarized waves are shown in Figs. 5(a) and 5(b) respectively. As it can be seen from Fig. 5(a), the magnitude of the reflection coefficient both for the *u*- and *v*-polarized waves is greater than −2.2 dB, while the phase difference between the *u*- and *v*-polarized reflected fields is 180° within the operating frequency band 5–15 GHz. Owing to the phase difference of 180° between the *u* and *v* components of the reflected electric field, an incident *x*-polarized wave is reflected as a *y*-polarized wave and vice versa (the principle is already explained using Fig. 2).

It is clear from Fig. 5 that the two resonances (dips in the reflection coefficient magnitude) occurring at 5.4 GHz and 12.4 GHz are due to the *u*-polarized incident wave, while the third resonance occurring at 7.6 GHz is due to the *v*-polarized incident wave. At resonance frequencies, the structure behave as an HIS for one component and a perfect electric conductor (PEC) for the other. The structural anisotropy along the *u*- and *v*-axes is an essential part of the design as it helps to provide a different electromagnetic response to the *u*- and *v*-polarized incident electric fields at the same frequency. The physical mechanism responsible for the CPC can be further understood by considering the surface current distribution on the top and bottom metallic surfaces for both the *u*- and *v*-polarized incident waves, as shown in Fig. 6. It is well known that, according to Faraday's law, a time changing magnetic field sandwiched between the two metals produces surface currents on the top and bottom metallic layers in opposite directions. As depicted in Fig. 6, the net current on the top and bottom layers (the ground plane) are directed in opposite directions at resonance frequencies. The vector sum of the currents is represented by the large black arrow and symbol $\boldsymbol{J}$ in Fig. 6. These oppositely directed currents on the top and bottom layers lead to a large value of magnetization producing high values for the anisotropic permeabilities μ_{uu} and μ_{vv}. Owing to the large impedance $\sqrt{\mu_{uu}/\varepsilon_{uu}}$, the surface behaved as an HIS at 5.4 and 12.4 GHz for the *u*-component of the electric field. Conversely, it acts as a normal electric conductor for the *v*-component at these frequencies. Similarly, the structure obtains magnetic resonance (large $\sqrt{\mu_{vv}/\varepsilon_{vv}}$) at 7.6 GHz only for the *v*-component of the incident electric field, behaving as a simple metallic reflector for the *u*-component.

At all three resonances, the metasurface acts as an HIS (reflecting with a 0° phase) for one component and as a normal metallic reflector (reflecting with a 180° phase) for the other, producing a 180° phase difference between the reflected field components leading to CPC.

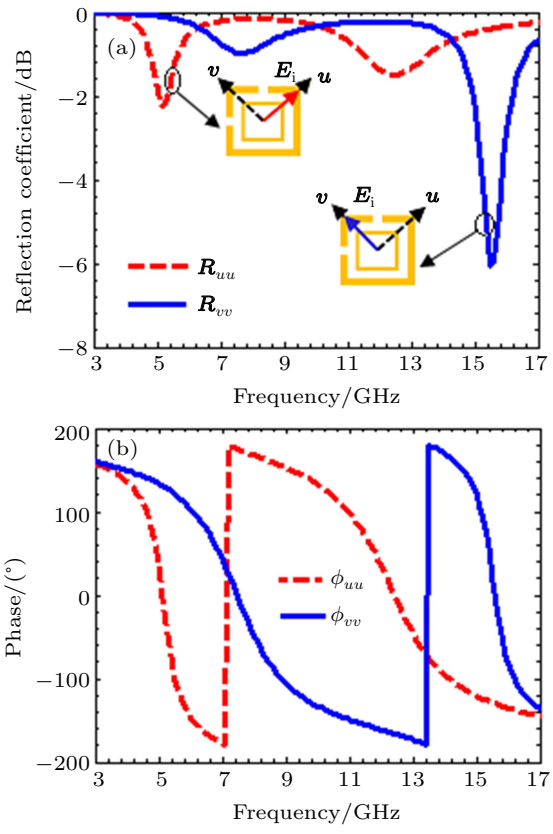


Fig. 5. (color online) Reflection coefficients: (a) magnitude and (b) phase, for *u* and *v*-polarized waves.

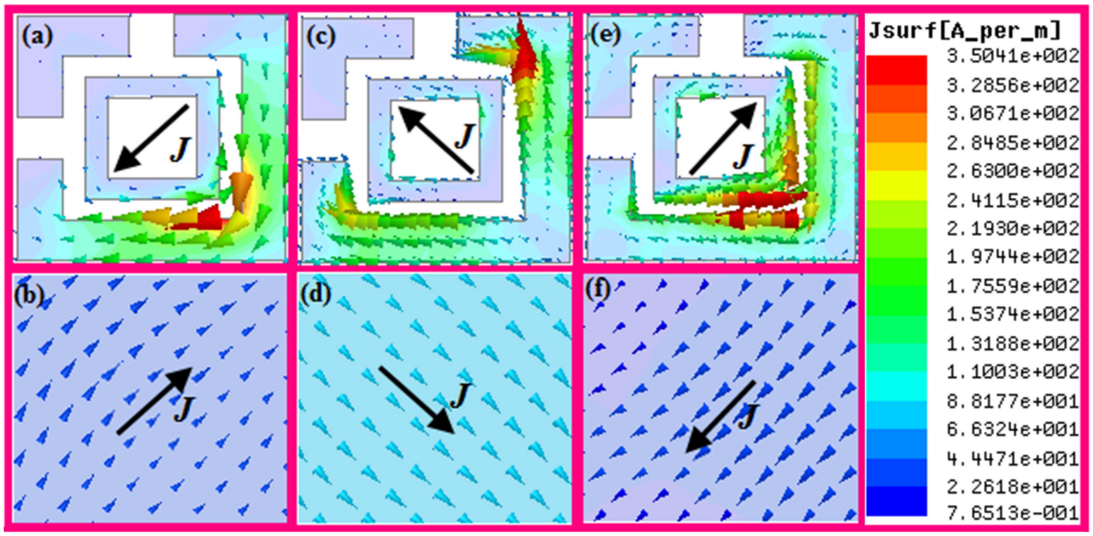


Fig. 6. (color online) Surface current distribution at resonant eigen-modes: 5.4 GHz ((a), (b)), 7.6 GHz ((c), (d)), 12.4 GHz ((e), (f)), on the top layer ((a), (c), (e)), and on ground plane ((b), (d), (f)).

Parametric analysis was carried out to investigate the effect of the geometrical dimensions on the response of the metasurface. Figure 7(a) presents the effect of varying the substrate thickness on the cross-polarized reflection coefficient. As it can be seen from Fig. 7(a), the cross-polarized reflection coefficient is small when the dielectric thickness is small. Furthermore, the bandwidth is also small for a small dielectric thickness. It can also be inferred from Fig. 7(a) that the optimum value for the substrate thickness is 2.4 mm.

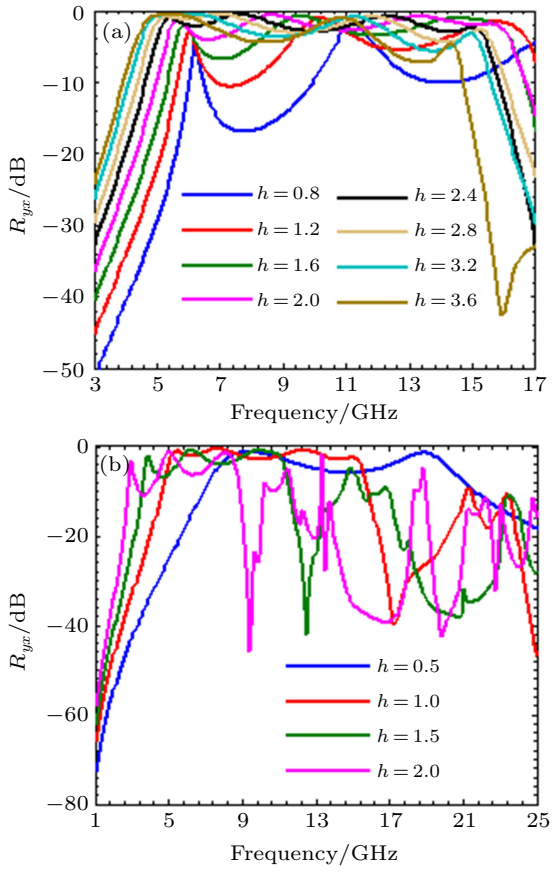


Fig. 7. (color online) Variation of the cross-polarized reflection coefficient when the (a) substrate thickness (h in mm) is varied and (b) geometrical dimensions in the xy-plane are scaled with a fixed substrate thickness of 2.4 mm.

The effect of changing the dimensions of the unit cell in the xy-plane on the cross-polarized reflection coefficient is also presented in Fig. 7(b). The geometrical dimensions of the unit cell are changed by scaling them in the xy-plane and keeping the substrate thickness fixed at 2.4 mm. All lengths and widths of the different parts of the unit cell in the xy-plane (given in section C) are halved, due to the scaling by 0.5. It can be seen from Fig. 7(b) that the response of the metasurface is shifted towards higher frequencies (blue shift) when the dimensions of the unit cell are reduced. Similarly, when the dimensions of the unit cell are increased by scaling with a number greater than one, the response is shifted towards lower frequencies (red shift). It is important to note that the periodicity of the unit cell must be far less than the operating wavelength to produce only specular reflections and avoid the scattering lobes. The ability to shift the response of the metasurface towards lower or higher frequencies by properly scaling the unit cell makes the proposed design a potential candidate for numerous applications in different frequency regimes.

3. Experimental verification

To validate the proposed design experimentally; a prototype of the metasurface was fabricated on a 305×305 mm^2 FR4 sheet on the top of which 44×44 unit cells were etched using standard PCB techniques. The FR4 sheet is backed by copper cladding. The measurements for the co- and cross-polarized reflection coefficients were carried out in an echoic chamber where the metasurface is illuminated by a one horn antenna, while the other horn antenna received the reflected wave. An Agilent N5232A was used for the measurement of

the received signals. The measurement setup is depicted in Fig. 8.

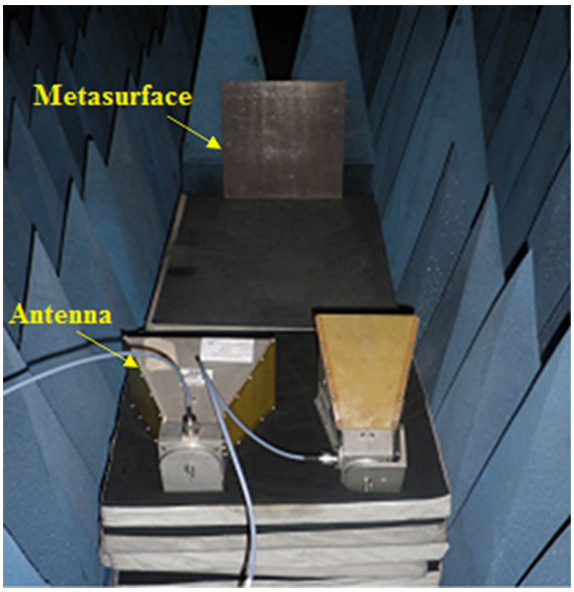


Fig. 8. (color online) Measurement setup.

For the measurement of the co-polarized reflection (R_{xx}), both of the antennas were placed in the horizontal orientation (x-polarization), while for R_{yy}, both were placed in the vertical orientation (y-polarization). For measuring the cross-polarized reflection R_{yx}, the transmitting antenna was placed in the horizontal orientation while the receiving antenna was placed in vertical orientation. Similarly, for R_{xy}, the transmitting antenna was placed in the vertical orientation while the receiving antenna was placed in the horizontal orientation. Figure 9 shows the simulation and measurement results for both the co- and cross-polarized reflection coefficients.

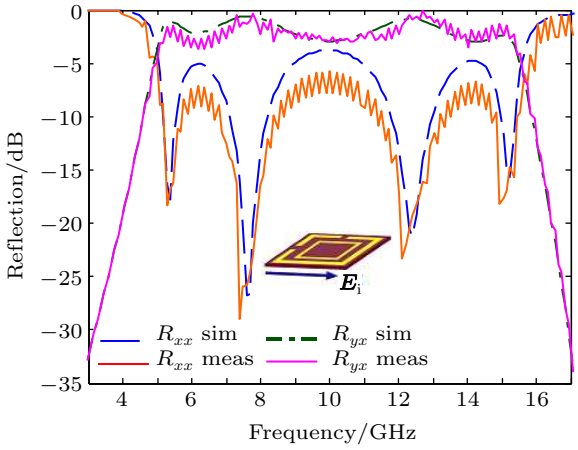


Fig. 9. (color online) Simulated and measured co- and cross-polarized reflection coefficients when the incident wave is x-polarized.

Figure 9 presents the results when the transmitting antenna transmitted the x-polarized wave while the receiving antenna was used to first receive the x-polarized (co-polarized) wave and then the y-polarized (cross-polarized) wave. The measurement results are in good agreement with the simulation results. The co- and cross-polarized reflections when the incident wave is y-polarized are presented in Fig. 10. The comparisons of the simulation and measurement results show that the measured results are consistent with the simulations. The small differences between the measured and simulated results are due to the fabrication imperfections and finite size of the fabricated sample.

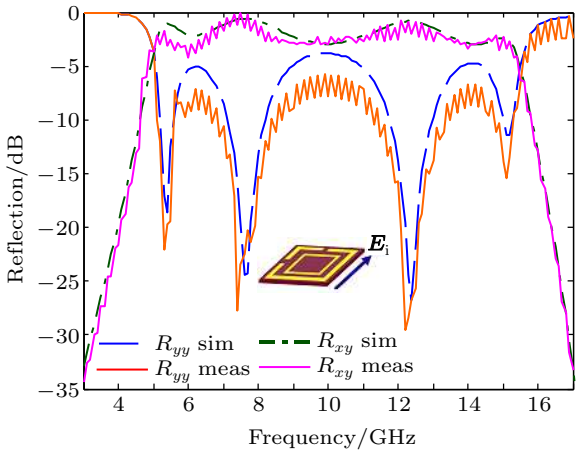


Fig. 10. (color online) Simulated and measured co- and cross-polarized reflection coefficients when the incident wave is y-polarized.

4. Conclusion

In summary, we have proposed and realized a thin ultra-wideband CPC metasurface working in the microwave regime. The designed metasurface converts an x-polarized wave into a y-polarized and vice versa over an ultra-broad frequency band from 5–15 GHz (10 GHz bandwidth). The broad bandwidth was realized through multiple plasmonic resonances and the polarization conversion efficiency reached 100%. Furthermore, the small sub-wavelength unit cell size (0.23λ at 10 GHz), thin dielectric substrate (0.08λ at 10 GHz), and overall optimized design of the unit cell resulted in a response of the metasurface that was insensitive to variations in the incidence angle up to 60°. The physical mechanism responsible for the polarization conversion was elucidated through the magnetic resonances and surface current distribution. The wide polarization conversion bandwidth and insensitivity to the incidence angle implies that the proposed metasurface is a potential candidate for many modern polarization control devices.

Acknowledgments

High recognition goes to the "Research Institute for Microwave and Millimeter-wave Studies (RIMMS)" at National University of Sciences and Technology, Islamabad, Pakistan. The authors acknowledge the support of RIMMS staff in fabrication and measurements of the metasurface.

References

[1] Saleh B E A and Teich M C 2007 *Fundamentals of Photonics* (New Jersey: Wiley)
[2] Veselago V G 1968 *Soviet Phys. Uspekhi* **10** 509
[3] Pendry J B 2000 *Phys. Rev. Lett.* **85** 3966
[4] Yu N and Capasso F 2014 *Nat. Mater.* **13** 139
[5] Qiong H E, Sun S L and Zhou L 2015 *Physics* **44** 366
[6] Hao J, Yuan Y, Ran L, Jiang T, Kong J A, Chan C T and Zhou L 2007 *Phys. Rev. Lett.* **99** 063908
[7] Pfeiffer C and Grbic A 2014 *Phys. Rev. Appl.* **2** 044011
[8] Xia R, Jing X, Gui X, Tian Y and Hong Z 2017 *Opt. Mater. Express* **7** 977
[9] Li R, Guo Z, Wang W, Zhang J, Zhang A, Liu J and Gao J 2014 *Opt. Express* **22** 27968
[10] Zhao Y, Cao X, Gao J, Liu X and Li S 2016 *Opt. Express* **24** 11208
[11] Song K, Liu Y, Luo C and Zhao X 2014 *J. Phys. D: App. Phys.* **47** 505104
[12] Ye Y and He S 2010 *Appl. Phys. Lett.* **96** 203501
[13] Khan M I, Fraz Q and Tahir F A 2017 *J. Appl. Phys.* **121** 045103
[14] Shi J H, Ma H F, Guan C Y, Wang Z P and Cui T J 2014 *Phys. Rev. B* **89** 165128
[15] Gao X, Yu X Y, Cao W P, Jiang Y N and Yu X H 2016 *Chin. Phys. B* **25** 128102
[16] Wu S, Huang X J, Xiao B X, Yan J and Yang H L Y 2014 *Chin. Phys. B* **23** 127805
[17] Zhu H L, Cheung S W, Chung K L and Yuk T I 2013 *IEEE Trans. Antennas Propag.* **61** 4615
[18] Yu N, Aieta F, Genevet P, Kats M A Gaburro Z and Capasso F 2012 *Nano Lett.* **12** 6328
[19] Doumanis E, Goussetis G, Gomez-Tornero J L, Cahill R and Fusco V 2012 *IEEE Trans. Antennas Propag.* **60** 212
[20] Grady N K, Heyes J E, Chowdhury D R, Zeng Y, Reiten M T, Azad A K and Chen H T 2013 *Science* **340** 1304
[21] Li Z, Mutlu M and Ozbay E 2014 *J. Phys. D: Appl. Phys.* **47** 075107
[22] Wang Y H, Shao J, Li J, Zhu M J, Li J, Zhou L and Dong Z G 2015 *J. Phys. D: Appl. Phys.* **48** 485306
[23] Tremain B, Rance H J, Hibbins A P and Sambles J R 2015 *Sci. Rep.* **5** 9366
[24] Chin J Y, Lu M and Cui T J 2008 *App. Phys. Lett.* **93** 251903
[25] Wei Z, Cao Y, Fan Y, Yu X and Li H 2011 *App. Phys. Lett.* **99** 221907
[26] Feng M, Wang J, Ma H, Mo W, Ye H and Qu S 2013 *J. Appl. Phys.* **114** 074508
[27] Chen H Y, Wang J F, Ma H, Qu S B, Zhang J Q, Xu Z and Zhang A X 2015 *Chin. Phys. B* **24** 014201
[28] Chen H, Wang J, Ma H, Qu S, Xu Z, Zhang A and Li Y 2014 *J Appl. Phys.* **115** 154504
[29] Ma H F, Wang G Z, Kong G S and Cui T J 2014 *Opt. Mat. Express* **4** 1717
[30] Shi H, Li J, Zhang A, Wang J and Xu Z 2014 *Opt. Express* **22** 20973
[31] Kuester E F, Mohamed M A, Piket-May M and Holloway C L 2003 *IEEE Trans. Antennas Propag.* **51** 2641
[32] Sievenpiper D, Zhang L, Broas R F, Alexopolous N G and Yablonovitch E 1999 *IEEE Trans. Microw. Theory Tech.* **47** 2059
[33] Menzel C, Rockstuhl C and Lederer F 2010 *Phys. Rev. A* **82** 053811
[34] Simovski C R, de Maagt P and Melchakova I V 2005 *IEEE Trans. Antennas Propag.* **53** 908
[35] De Cos M E and Las-Heras F 2015 *Appl. Phys. A* **118** 699